Applied Biological Research 21(1): 49-57; (2019)
DOI: 10.5958/0974-4517.2019.00010.7

ANALYSIS OF SKIN LESIONS USING GMM-HMRF REGION-BASED SEGMENTATION TECHNIQUE

Sudhakar Singh[1] and Shabana Urooj[2]

Department of Electrical Engineering, School of Engineering, Gautam Buddha University, Greater Noida – 201312, Uttar Pradesh (India)
*e mail: *[1]) sudhakarsingh86@gmail.com, [2]) shabanaurooj@ieee.org*

(Received 10 August, 2018; accepted 18 December, 2018)

ABSTRACT

This paper was aimed to develop a computer-aided detection (CAD) system which may support dermatologists in their early diagnosis of skin cancer from dermoscopic images. Segmentation play key role in the automatic detection of skin lesions. In this paper Gaussian Mixture Model-based Hidden Markov Random Field (GMM-HMRF) region-based segmentation method was used. The technique is fast and automated for dermoscopic images and is used in quantitative experimental analysis for publicly available data base and compared with two other well-known methods. The results revealed that the proposed method was highly accurate. The proposed segmentation technique achieved remarkable results for nevus images [accuracy (ACC) = 97.21%, sensitivity (SE) = 95.43% and specificity (SP) = 91.76%]; while for benign images (ACC = 96.15%, SE = 96.26% and SP = 95.32) and basal cell carcinoma & Seborrheic keratoses images (ACC = 96.85%, SE = 96.85% and SP = 97.34) the results were almost same.

Key words: Feature extraction, fuzzy C-mean, GMM-HMRF, segmentation

INTRODUCTION

Most violent tumor in humans is melanoma (Celebi *et al*., 2009; Marchetti *et al.*, 2017) and is often fatal if unnoticed in time. The frequency of melanoma is 4% amongst the all dermatologic diseases (Sadeghi, *et al*., 2012). Further, the assured skin cancers cases have 80% chances of death and only 14% patients with metastatic melanoma can persist up to 5 years. The malignant melanoma has >95% cure rate if noticed in early phase (Sadeghi, *et al*., 2012). Hence, there is an urgent need to develop improved methods which may improve diagnostic precision and help dermatologists in early detection as it is the only way to reduce death chances from melanoma (Abbas *et al*., 2013). Dermoscopy is a vital tool in the initial analysis of melanoma. Dermoscopy images are formed by uniting optical magnification by any liquid immersion or cross polarized lighting (Barata *et al*., 2014), with a low angle-of-incidence lighting (Abbas *et al*., 2013). Dermoscopy images provide amplification of lesions thus ensure better analysis of specific features of lesion with respect to symmetry, border, size and distribution of colour. An automatic computer-aided diagnostic (CAD) system consists of 4 parts involved in i) acquisition of image, ii. image filtering, iii. segmentation of lesion, and iv. classification (Huang *et al.*, 2013). Segmentation section is very important which can muscularly affect the accuracy of CAD system (Barata *et al*., 2015; Abbas *et al.*, 2017). Irregularity and border information are also important for lesion diagnosis. Segmentation permits the removal of the area of interest of an image (Sadri *et al.*, 2013; Barata *et al*., 2016). So proper segmentation of skin lesion is essential for analysis because several artifacts like hairs, shadow, bubble, skin lines

and reflections might affect the accuracy (Übeyli, 2009). The result obtained by GMM-HMRF segmentation are reportedly smoother than those of direct Fuzzy C-means and Otsu methods.

Threshold based segmentation technique are histogram thresholding (Pirnog *et al.,* 2015; Celebi and Mishra, 2016), adaptive thresholding (Wang *et al.,* 2011) and clustering. Dissimilar thresholding approaches can be united together. In region-based techniques pixel-approaches are used in grouping through a region-growing method for automatically removing the lesion of dermoscopy image (Bagci *et al.,* 2013). Four techniques are measured for the construction of ensemble: i) maximum entropy, ii) fuzzy likeness, iii) Otsu's clustering and iv) minimum error thresholding (Singh *et al.,* 2018). The performance of thresholding technique is better if there is greater difference between adjacent skin region and lesion area, otherwise the segmentation precision may decline. Thresholding approaches can flop when images with major extent of hair or bubbles (Cremers *et al.* 2007).

Edge and contour approach deals with the edges or discontinuity of dermoscopic images. An active contour method, created on gradient vector flow (GVF) snakes for contour extraction, is defined by Sadeghi *et al.* (2012). An improvement of GVF built on mean shift (MSGVF) was developed by Wang (2012b). Both active contour and adaptive snake techniques are applied for the segmentation of skin lesion (Silveira *et al.,* 2009). Edges are mainly gathered in strokes and then each stroke is classified in adaptive snake algorithm (Wang *et al.,* 2011; Yu *et al.,* 2017). Each stroke contains confidence level and expectation-maximization (EM) algorithm is applied for the confidence levels to evaluate the object contour. The active contour through level set technique has also been demonstrated (Arbeláez *et al.,* 2011; Pirnog *et al.,* 2015). Edge and contour-based methods usually fail in the attendance of air bubbles or hair and when the changeover between lesion and the nearby is even.

Scanty information is available on region-based segmentation which assumes that any image has two regions: i) skin, and ii) lesion. Spatial segmentation and colour quantization, also called JSEG technique, has been employed for the segmentation of skin lesion images (Cremers *et al.,* 2007). Statistical region merging (SRM) technique is also employed (Scharfenberger *et al.,* 2013) and it gives the image as detected case of an unidentified hypothetical image whose geometric areas are to be recreated. The present study was aimed to develop a computer-aided detection system, using region-based segmentation technique, which may support dermatologists in their early diagnosis of skin cancer from dermoscopic images.

MATERIALS AND METHODS

GMM-based HMRF

Markov random field's (MRFs) technique is widely used in image processing issues like image segmentation (Wang, 2012a), surface reconstruction (Grady, 2006), depth logical thinking (Glaister *et al.,* 2014), etc. Its success is attributed to the economical algorithms such as iterated conditional modes (Eigen *et al.,* 2014), and it's thought of each "data faithfulness" and "model smoothness" (Wang, 2012b). HMRF-EM method was initially proposed for segmentation of brain MRI pictures (Zhang *et al.,* 2001). For simplicity, it is assumed that intensity distribution of every region to be segmental follows a normal distribution of 2D gray-level image.

A picture is bestowed as $Y = (y_1 \ldots. y_N)$ wherein N is the number of pixels and y_i is the concentration of gray-level of a pixel. The configuration of labels is outlined as $X = (x_1, \ldots, x_N)$ where $l \in L$ and L are that the set of all probable labels. During a binary segmentation downside, $L = \{0, 1\}$. Here X is label then MAP measure satisfies:

$$X = \arg\max_{X}\{P(Y / X)P(X)\} \quad \ldots\ldots\ldots \quad (1)$$

Here former probability P(X) is a Gibbs distribution, and the combined likelihood probability is:

$$P(Y/X,\theta)=\prod_i P(y_i/X,\theta) \;=\; \prod_i P(y_i/x_i,\theta_{xi}) \qquad \ldots\ldots\ldots \qquad (2)$$

where $P(y_i/x_i,\theta_{xi})$ is Gaussian distribution with parameters $\theta_{xi}=(\mu_{xi},\sigma_{xi})$ and $\theta = \{\theta_l \,|l\in L\}$ as learning parameters.

The intensity scattering of every region follows a normal distribution with parameters $\theta_{xi}=(\mu_{xi},\sigma_{xi})$. However, this can really be a robust hypothesis that is meant to model the complexness of intensity distribution of real-life objects, particularly those with multimodal distribution. Gaussian mixture model (GMM), in distinction, is additional authoritative for modeling complicated distributions than one single Gaussian distribution. A Gaussian mixture model with 'g' parts is drawn by parameters:

$$\theta_l=\left\{(\mu_{l,1},\sigma_{l,1},w_{l,1}).....,(\mu_{l,g},\sigma_{l,g},w_{l,g})\right\} \qquad \ldots\ldots \qquad (3)$$

Compared with Eq. (7), the GMM now has a weighted probability. After comparison between Gaussian mixture model and Gaussian distribution function Eq. (4) is formed given as below.

$$G_{mix}(z,\theta_l)=\sum_{c=1}^{g} G\left(z;\ \mu_{l,c},\ \sigma_{l,c}\right) \qquad \ldots\ldots\ldots \qquad (4)$$

Now, the M-step of EM-algorithm delineate below for Gaussian mixture model fitting downside. The GMM fitting downside itself is additionally solved by means of associate in Nursing EM-algorithm. E-step confirm that the information ought to belong to Gaussian components, then M-step further calculates the GMM parameters.

Expectation maximization (EM) algorithm for parameters

In the proposed algorithm, 2-D gray-level and Gaussian distribution assumption have been used. The EM- formula was used to estimate the parameter set $\theta = \{\theta_l \,|l \in L\}$. EM algorithm can be defined as:

1. It is assumed initial parameter $\theta^{(0)}$.
2. E-step: Conditional expectation at t[th] iteration, calculated as:

$$Q(\theta/\theta^{(t)})=E[\ln P(X,Y/\theta)/Y,\theta^{(0)}]=\sum_{X\varepsilon x} P(X,Y/\theta^{(t)})\ln P(X,Y/\theta) \ldots\ldots \qquad (5)$$

Here X is the set of all probable formations of labels.

3. M-step: To maximize $Q(\theta/\theta^{(t)})$ to get the subsequent estimate:

$$\theta^{(t+1)}=\arg\max_x Q(\theta/\theta^{(t)}) \qquad \ldots\ldots\ldots\ldots \qquad (6)$$

Then let $\theta^{(t+1)}\rightarrow\theta^{(t)}$ and repeat from the E-step.

Assumed $G(z,\theta_l)$ is a Gaussian distribution function having parameters $\theta_l=(\mu_l,\sigma_l)$:

$$G(z,\theta_l)=\frac{1}{\sqrt{2\pi\varsigma_l^2}}\exp(-\frac{(z-\mu_l)^2}{2\sigma_l^2}) \qquad \ldots\ldots\ldots\ldots \qquad (7)$$

And the previous probability can be presented as

$$P(X)=\frac{1}{Z}\exp(-U(X) \qquad \ldots\ldots\ldots\ldots \qquad (8)$$

where $U(X)$ is the previous energy function; and

$$P(Y/X,\theta)=\prod_i P(y_i/x_{i,}\theta_{xi}) \;=\; \prod_i G(y_i,\theta_{xi}) \qquad \ldots\ldots\ldots\ldots \qquad (9)$$

With these assumptions, the HMRF-EM algorithm is given below:

1. Start with first parameter set $\theta^{(0)}$.
2. Compute the probability distribution $P^{(t)}(y_i/x_i,\theta_{xi})$.
3. With present parameter set $\theta^{(t)}$ to calculate the labels by MAP estimation:

$$X^{(t)}=\arg\max_{X\varepsilon x}\{P(Y/X,\theta^{(t)})P(X)\} \;=\; \arg\max_{X\varepsilon x}\{U(Y/X,\theta^{(t)})+U(X)\} \ldots\ldots \qquad (10)$$

4. Calculate the posterior distribution using Bayesian rule for all l ∈ L and all pixels y_i:

$$P^{(t)}(l / y_i) = \frac{Z(y_{i,}\theta_l)P(l / x_{N_i}^{(t)})}{P^{(t)}(y_i)} \quad \ldots\ldots\ldots \quad (11)$$

where $x_{N_i}^{(t)}$ is the neighborhood configuration of $x_i^{(t)}$, and

$$P^{(t)}(y_i) = \sum_{l\varepsilon L} G(y_{i,}\theta_l)P(l / x_{N_i}^{(t)}) \quad \ldots\ldots\ldots \quad (12)$$

Note here $P(l / x_{N_i}^{(t)}) = \frac{1}{Z}\exp(\sum_{j\varepsilon N_i} V_c(l, x_j^{(t)}))$ ……. (13)

To update the parameters, use $P^{(t)}(l / y_i)$:

$$\mu_l^{t+1} = \frac{\sum_i P^{(t)}(l / y_i)y_i}{\sum_i P^{(t)}(l / y_i)} \quad \ldots\ldots\ldots \quad (14)$$

$$(\sigma_l^{(t+1)})^2 = \frac{P^{(t)}(l / y_i)(y_i - \mu_l^{t+1})^2}{P^{(t)}(l / y_i)} \quad \ldots\ldots\ldots \quad (15)$$

Maximum A Posteriori (MAP) estimation for labels

In EM algorithm, to solve for X that minimizes the entire posterior energy

$$X = \arg\max_{X\varepsilon x}\{U(Y / X, \theta) + U(X)\} \quad \ldots\ldots\ldots \quad (16)$$

with given Y and θ, where the probability energy (unitary potential) is:

$$U(Y / X, \theta) = \sum_i U(y_i / x_i, \theta) = \frac{\sum_i (y_i - \mu_{x_i})^2}{2\sigma_{x_i}^2} + \ln\sigma \quad \ldots\ldots\ldots \quad (17)$$

The past energy function (also called pairwise potential)

$$U(X) = \sum_{c\varepsilon C} Vc(X) \quad \ldots\ldots\ldots \quad (18)$$

Here Vc(X) is the clique potential and 'c' is that the set of all potential cliques. For image domain, one picture element has at the most four neighbours. The clique potential is calculated on couples of neighboring pixels:

$$Vc(x_{i,}x_j) = \frac{1}{2}(1 - I_{x_1, x_j}) \quad \ldots\ldots\ldots\ldots\ldots \quad (19)$$

where I_{x_i, x_j} = 0, if x_i is not equal to x_j

= 1, if x_i = x_j .

Note in Eq. (17) the constant coefficient 1/2 can be replaced by a variable coefficient β. Follow Zhang *et al.* (2001) to use the 1/2 constant that proves effective in several experiment results.

For solving the equation (17) an iterative algorithm is proposed as below:

1. Start using an initial value $X^{(0)}$ that can be from the previous loop of EM algorithm.
2. Provided X(k), for all 1 ≤ i ≤ N, we find

$$x_i^{(k+1)} = \arg\max_{l\varepsilon L}\{U(y_i / l) + \sum_{j\varepsilon N_i} V_c(l, x_j^{(k)})\} \quad \ldots\ldots\ldots\ldots \quad (20)$$

3. Repeat step 2 till $U(Y / X, \theta) + U(X)$ stops varying meaningfully or an extreme k is attained.

Lesion segmentation

The dissimilarity between colour image and gray-level image segmentation is that for a colour picture the pixel intensity is no longer a numeral, however a 3-dimensional vector of RGB standards: Y = (y_1; : : : ; y_N), and y_i = (y_{iR}; y_{iG}; y_{iB})^T. The Gaussian mixture model now develops:

$$\theta_l =, \{(\mu_{l,1,}\Sigma_{l,1}, w_{l,1}), \ldots\ldots, (\mu_{l,g,}\Sigma_{l,g}, w_{l,g})\} \quad \ldots\ldots\ldots\ldots \quad (21)$$

Which can be compared with Eq. (10). Also, the likelihood energy Eq. (17) becomes

$$U(Y / X, \theta) = \sum_i U(y_i / x_i, \theta) = \sum_i \left[\frac{1}{2}(y_i - \mu_{x_i})^T \sum_{x_i}^{-1}(y_i - \mu_{x_i}) + \ln|\Sigma_{x_i}|^{\frac{1}{2}}\right] \quad \ldots. \quad (22)$$

RESULTS AND DISCUSSION

Qualitative analysis

The international skin imaging collaboration (ISIC) (Marchetti *et al.*, 2017) is an academia-industry partnership intended to facilitate digital skin imaging technologies to help in reducing the melanoma mortality. In this study, 200 images were used from a data set of 1200 images. The results obtained by the proposed technique showed better segmentation as compared to other two segmentation techniques. The obtained segmented images were smoother than those obtained by other two techniques and the region of lesions segmented out better than other two techniques (Fig. 1). Obtained segmented image were close to ground truth.

Quantitative analysis

For quantitative analysis two other techniques used were Otsu and fuzzy c-means segmentation techniques that are based on thresholding; while the proposed technique is region-based. To acquire segmentation results, three completely different metrics namely accuracy, sensitivity and specificity segmentation results, three completely different metrics namely accuracy, sensitivity and specificity

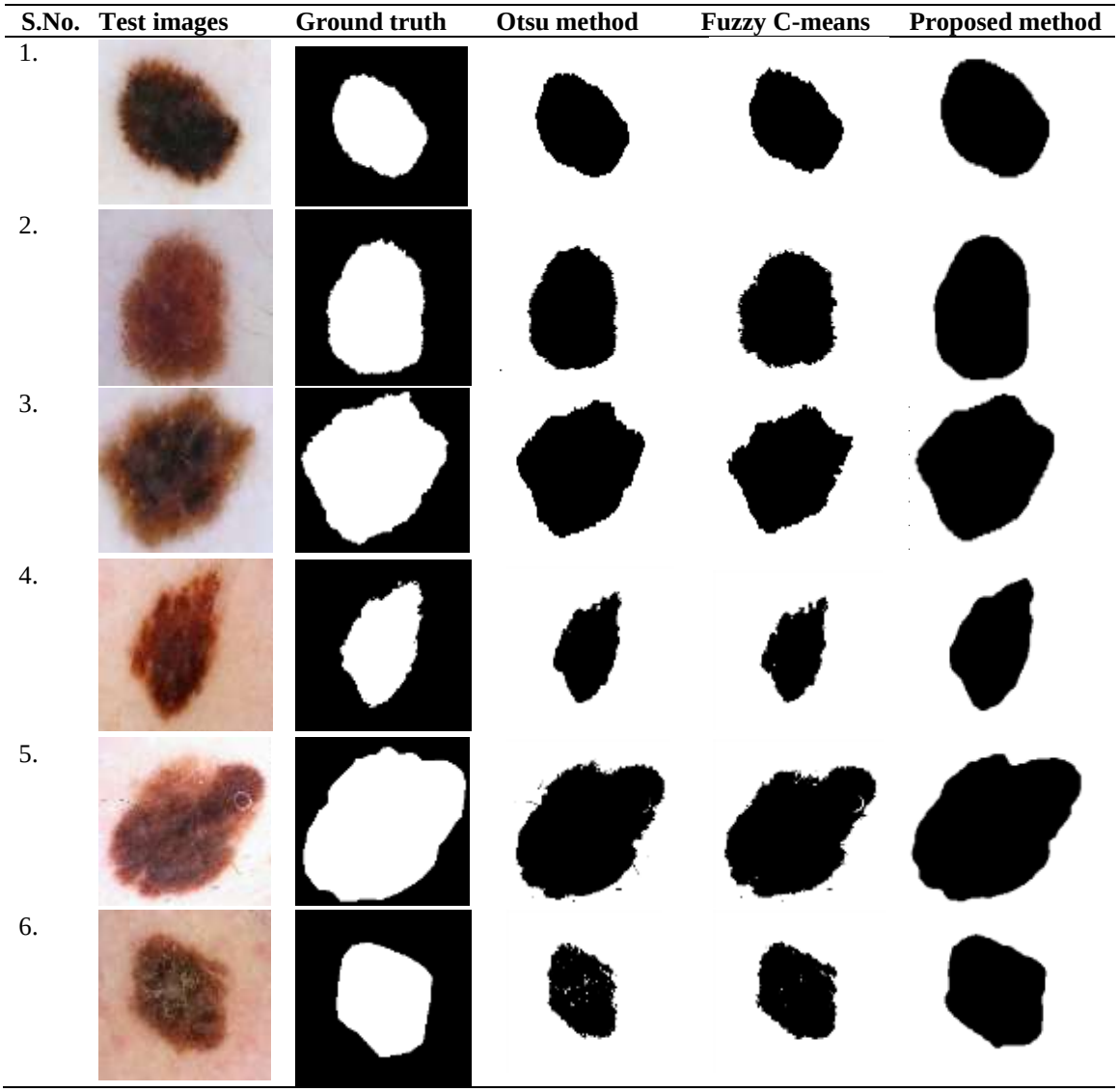

Fig. 1: Comparison of different segmentation techniques

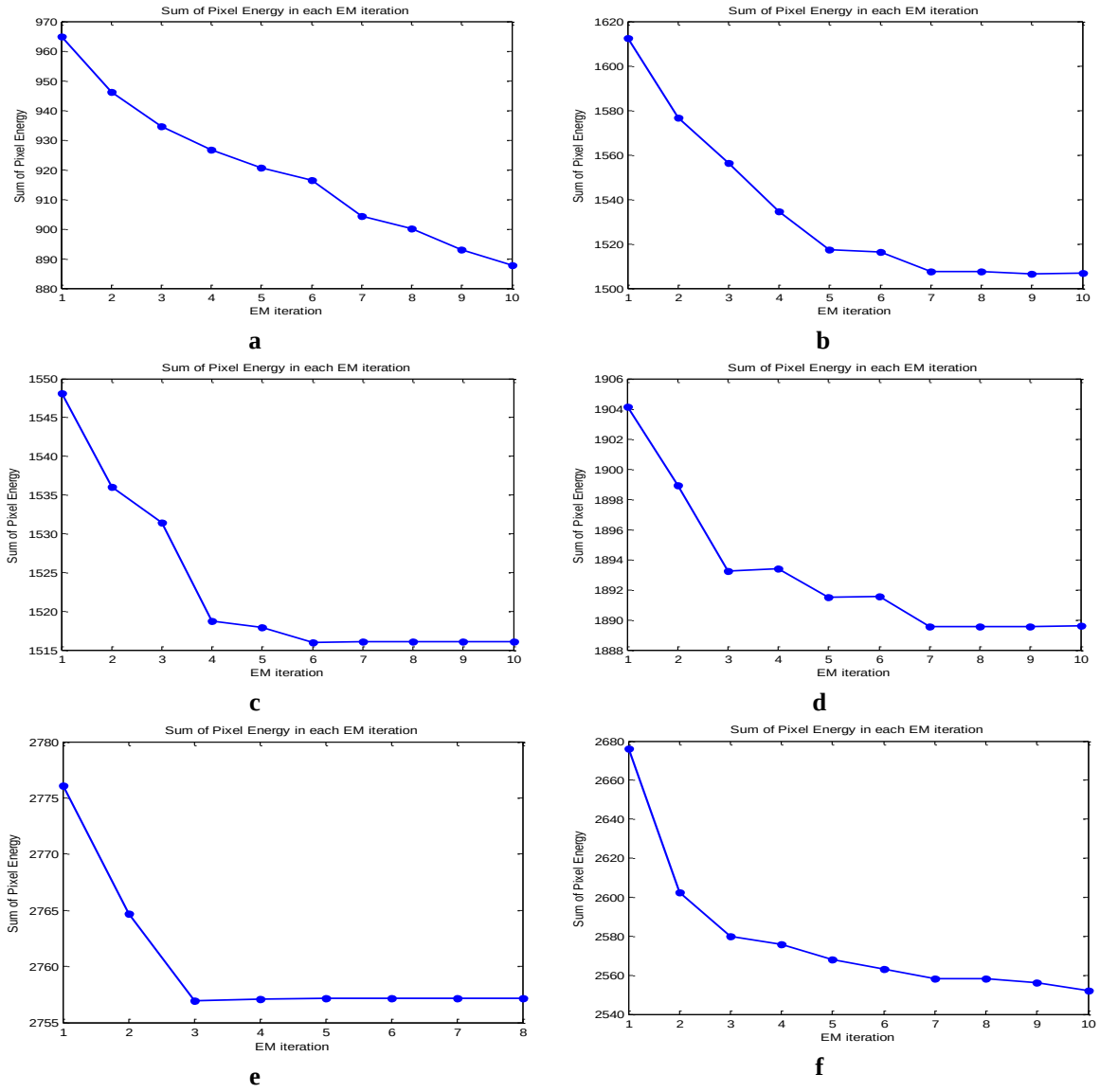

Fig. 2: Graph of the sum of pixels energy vs EM iterations of all six test images

were computed. Fig. 2 displays the graph of sum of pixels energy versus EM iterations for all six test images. It presents the energy v/s expectation-maximization (EM) iteration for all the six test images. The definitions for the used metrics are given in the below given equations, wherever TP is the range of true positive pixels, FP is the range of false positive pixels, TN is the range of true negative pixels, and FN is the range of false negative pixels. The chosen metrics are extensively used in literature to compute the performance of skin lesion segmentation strategies. Each formula is applied to the corrected pictures and the consequent segmentation is compared with the manually drawn segmentation which serves as ground truth. The metrics-accustomed compared with ground truth square measure sensitivity, specificity, and accuracy.

$$\text{Sensitivity} = \frac{TP}{TP + FN}$$

$$\text{Specificity} = \frac{TN}{TN + FP}$$

$$\text{Accuracy} = \frac{TN + TP}{TN + TP + FN + FP}$$

Table 1: Segmentation result metrics of malignant melanoma, benign melanoma, nerves, basal cell carcinoma and seborrheic keratoses

Techniques	Accuracy (%)	Sensitivity (%)	Specificity (%)
Malignant melanoma (75 images)			
Fuzzy c-means	92.76	90.43	87.32
Otsu-RGB	93.65	94.21	86.36
Proposed	96.23	93.40	93.76
Benign melanoma (60 images)			
Fuzzy c-means	93.32	95.65	92.43
Otsu-RGB	95.23	94.87	86.34
Proposed	96.15	96.26	95.32
Nevus (58 images)			
Fuzzy c-means	91.21	90.25	94.35
Otsu-RGB	94.34	92.52	91.38
Proposed	97.21	95.43	91.76
Basal cell carcinoma (42 images)			
Fuzzy c-means	95.34	95.76	96.23
Otsu-RGB	95.64	94.34	95.12
Proposed	96.85	96.85	97.34
Seborrheic keratoses (45 images)			
Fuzzy c-means	93.34	95.76	96.23
Otsu-RGB	94.58	94.34	95.12
Proposed	96.85	96.85	97.34

The attained result metrics for 75 malignant melanoma using the proposed technique had sensitivity of 93.4%, specificity of 93.76% and accuracy of 96.23% which was better than the other two techniques (Table 1). In case of benign melanoma images, the proposed segmentation technique had 96.26% sensitivity, 95.32% specificity, and 96.15% accuracy. Similarly, proposed technique for 58 nevus images showed 97.21% accuracy, 95.43% sensitivity, and 91.76% specificity and was better than other two techniques. In case of basal cell carcinoma image, the proposed segmentation technique showed 96.85% accuracy and specificity and 97.34% sensitivity and proved better than other techniques tested. The segmentation results of proposed technique for 45 Seborrheic keratoses images had 96.85% accuracy and sensitivity 96.85% and 97.34% specificity which was better than other two techniques.

Conclusion: The quantitative investigation of the performance of proposed method was carried out by considering three different metrics. The segmentation results were better than ground truth data in case of nevus images, whereas the segmentation precision for the rest images were nearly same. The simulation results reveal that the proposed approach gives additional correct skin lesion segmentation results than comparable progressive strategies. Consequently, the projected segmentation methodology may be used in clinical skin lesion pre-screening systems to assist the rising accuracy of early carcinoma identification, which might have an effect on absolute prognosis of carcinoma patients, and finally scale back the prices associated to health care.

REFERENCES

Abbas, Q., Agarwal, A., Issac, A., Dutta, M.K., Doneva, V., Ivanovski, Z., and Scharcanski, J. 2017. Skin lesion segmentation based on preprocessing, thresholding and neural networks. *Expert Systems with Applications*. [*https://doi.org/10.1088/1742-6596/755/1/011001*].

Abbas, Q., Garcia, I.F., Emre Celebi, M., Ahmad, W. and Mushtaq, Q. 2013. A perceptually oriented method for contrast enhancement and segmentation of dermoscopy images. *Skin Research and Technology*, **19** (1). [*https://doi.org/10.1111/j.1600-0846.2012.00670.x*].

Arbeláez, P., Maire, M., Fowlkes, C. and Malik, J. 2011. Contour detection and hierarchical image segmentation. *IEEE Transactions on Pattern Analysis and Machine Intelligence*, **33:** 898-916.

Bagci, U., Udupa, J.K., Mendhiratta, N., Foster, B., Xu, Z., Yao, J. and Mollura, D.J. 2013. Joint segmentation of anatomical and functional images: Applications in quantification of lesions from PET, PET-CT, MRI-PET, and MRI-PET-CT images. *Medical Image Analysis*, **17:** 929-945.

Barata, C., Celebi, M.E. and Marques, J.S. 2015. Improving dermoscopy image classification using color constancy. *IEEE Journal of Biomedical and Health Informatics*, **19:** 1146-1152.

Barata, C., Celebi, M.E., Marques, J.S. and Rozeira, J. 2016. Clinically inspired analysis of dermoscopy images using a generative model. *Computer Vision and Image Understanding*, **151:** 124-137.

Barata, C., Ruela, M., Francisco, M., Mendonca, T. and Marques, J.S. 2014. Two systems for the detection of melanomas in dermoscopy images using texture and color features. *IEEE Systems Journal*, **8:** 965-979.

Celebi, M.E., Iyatomi, H., Schaefer, G. and Stoecker, W.V. 2009. Lesion border detection in dermoscopy images. *Computerized Medical Imaging and Graphics : The Official Journal of the Computerized Medical Imaging Society*, **33:** 148-153.

Celebi, M.E. and Mishra, N.K. 2016. An overview of melanoma detection in dermoscopy images using image in processing and machine learning. *Arxiv Statistics - Machine Learning*, 1-15. [*https://doi.org/https://arxiv.org/abs/1601.07843v1*].

Cremers, D., Rousson, M. and Deriche, R. 2007. A review of statistical approaches to level set segmentation: Integrating color, texture, motion and shape. *International Journal of Computer Vision*, **72:** 195-215.

Eigen, D., Puhrsch, C. and Fergus, R. 2014. Depth map prediction from a single image using a multi-scale deep network. *NIPS*, 1–9. [*https://doi.org/10.1007/978-3-540-28650-9_5*].

Glaister, J., Wong, A. and Clausi, D.A. 2014. Segmentation of skin lesions from digital images using joint statistical texture distinctiveness. *IEEE Transactions on Biomedical Engineering*, **61:** 1220-1230.

Grady, L. 2006. Random walks for image segmentation. *Pattern Analysis and Machine Intelligence, IEEE Transactions On*, **28:** 1768-1783.

Huang, A., Kwan, S.Y., Chang, W.Y., Liu, M.Y., Chi, M.H. and Chen, G.S. 2013. A robust hair segmentation and removal approach for clinical images of skin lesions. pp. 3315-3318. **In**: *Proceedings of the Annual International Conference of the IEEE Engineering in Medicine and Biology Society, EMBS* [*https://doi.org/10.1109/EMBC.2013.6610250*].

Marchetti, M.A., Codella, N.C.F., Dusza, S.W., Gutman, D.A., Helba, B., Kalloo, A., Mishra, N., Carrera, C., Celebi, M.E., DeFazio, J., Jaimes, N, Marghoob, A.A., Quigley, E., Scope, A., Yelamos, O. and Halpern, A.C. 2017. Results of the 2016 international skin imaging collaboration international symposium on biomedical imaging challenge: Comparison of the accuracy of computer algorithms to dermatologists for the diagnosis of melanoma from dermoscopic images. *Journal of the American Academy of Dermatology*. [*https://doi.org/10.1016/j.jaad.2017.08.016*]

Pirnog, I., Preda, R.O., Oprea, C. and Paleologu, C. 2015. Automatic lesion segmentation for melanoma diagnostics in macroscopic images. pp. 659-663. **In**: *23rd European Signal Processing Conference, EUSIPCO 2015*. [*https://doi.org/10.1109/EUSIPCO.2015.7362465*].

Sadeghi, M., Lee, T.K., Mclean, D., Lui, H. and Atkins, M.S. 2012. Oriented pattern analysis for streak detection in dermoscopy images. pp. 298-306. **In**: *MICCAI: International Conference on Medical Image Computing and Computer-Assisted Intervention. 15th Internaltional Conference, Proceedings Part 1*. 1-5 October, 2012, Nice, France.

Sadri, A.R., Zekri, M., Sadri, S., Gheissari, N., Mokhtari, M. and Kolahdouzan, F. 2013. Segmentation of dermoscopy images using wavelet networks. *IEEE Transactions on Biomedical Engineering*, **60:** 1134-1141.

Scharfenberger, C., Wong, A., Fergani, K., Zelek, J.S. and Clausi, D.A. 2013. Statistical textural distinctiveness for salient region detection in natural images. **pp**. **979-986. In**: *Proceedings of the IEEE Computer Society Conference on Computer Vision and Pattern Recognition*, CVPR, June 2013. [*https://doi.org/10.1109/CVPR.2013.131*].

Silveira, M., Nascimento, J.C., Marques, J.S., Marçal, A.R.S., Mendonça, T., Yamauchi, S. and Rozeira, J. 2009. Comparison of segmentation methods for melanoma diagnosis in dermoscopy images. *IEEE Journal on Selected Topics in Signal Processing*, **3:** 35-45.

Singh, S., Urooj, S. and Singh, S.P. 2018. Analysis of leukoderma images using neuro-fuzzy hybrid technique. pp. 93-101. **In**: *Sensors and Image Processing: Advances in Intelligent Systems and Computing*, volume 651. Springer, Singapore.

Übeyli, E.D. 2009. Combined neural networks for diagnosis of erythemato-squamous diseases. *Expert Systems with Applications*, **36:** 5107-5112.

Wang, H., Moss, R.H., Chen, X., Stanley, R.J., Stoecker, W.V., Celebi, M.E. and Szalapski, T.M. 2011. Modified watershed technique and post-processing for segmentation of skin lesions in dermoscopy images. *Computerized Medical Imaging and Graphics*, **35:** 116-120.

Wang, Q. 2012a. GMM-based hidden Markov random field for colour image and 3D volume segmentation. *ArXiv Preprint ArXiv:1212.4527*, **1:** 1-7. [*http://arxiv.org/abs/1212.4527*].

Wang, Q. 2012b. HMRF-EM-image: Implementation of the hidden Markov random field model and its expectation-maximization algorithm. *ArXiv Preprint ArXiv:1207.3510*, **5**: 5-8. [*http://arxiv.org/abs/1207.3510*].

Yu, L., Chen, H., Dou, Q., Qin, J. and Heng, P.A. 2017. Automated melanoma recognition in dermoscopy images via very deep residual networks. *IEEE Transactions on Medical Imaging*, **36:** 994-1004.

Zhang, Y., Brady, M. and Smith, S.M. 2001. Segmentation of brain MR images through a hidden Markov random field model and the expectation-maximization algorithm. *IEEE Transactions on Medical Imaging*, **20:** 45-57.